Dalton Transactions

PAPER

View Article Online
View Journal | View Issue

Cite this: *Dalton Trans.*, 2018, **47**, 15827

Humidity-induced CO_2 capture enhancement in Mg-CUK-1†

Mónica Sagastuy-Breña,‡[a] Paulo G. M. Mileo,‡[b] Elí Sánchez-González,[a] Joseph E. Reynolds, III,[c] Tamara Jurado-Vázquez,[a] Jorge Balmaseda,[a] Eduardo González-Zamora,[d] Sabine Devautour-Vinot,[b] Simon M. Humphrey,*[c] Guillaume Maurin*[b] and Ilich A. Ibarra*[a]

Received 17th August 2018,
Accepted 19th October 2018

DOI: 10.1039/c8dt03365j

rsc.li/dalton

Kinetic CO_2 adsorption measurements in the water-stable and permanently microporous Metal–organic framework material, Mg-CUK-1, reveal a 1.8-fold increase in CO_2 capture from 4.6 wt% to 8.5 wt% in the presence of 18% relative humidity. Thermodynamic CO_2 uptake experiments corroborate this enhancement effect, while grand canonical Monte Carlo simulations also support the phenomenon of a humidity-induced increase in the CO_2 sorption capacity in Mg-CUK-1. Molecular simulations were implemented to gain insight into the microscopic adsorption mechanism responsible for the observed CO_2 sorption enhancement. These simulations indicate that the cause of increasing CO_2 adsorption enthalpy in the presence of H_2O is due to favorable intermolecular interactions between the co-adsorbates confined within the micropores of Mg-CUK-1.

Introduction

The continuous rising levels of atmospheric carbon dioxide that result from anthropogenic emissions is one of the greatest environmental threats to our civilization. For example, in 2017, worldwide CO_2 emissions from fossil fuel combustion increased by about 2% compared to the previous two years.[1] Such a dramatic increase contributed to the current total world record of 36.8 Gt of CO_2 in the atmosphere.[2] Undoubtedly, identifying ways to significantly reduce atmospheric CO_2 levels is critical to alleviate the threat that global warming presents to our planet. At present, national governments are working together on a world-wide basis to promote the development of new technologies for more efficient and effective CO_2 capture.[3] In addition to existing CO_2 capture technologies (*e.g.* alkanolamine aqueous solutions or alkaline solid adsorbents), potential replacement technologies are currently being investigated at a more fundamental level. This includes the use of porous solid-state materials for adsorption–desorption based processes.[4] Therefore, new porous materials with high chemical and thermal stability, high CO_2 adsorption capacities, and that enable fast CO_2 sorption kinetics and desorption under mild conditions, are actively being sought.[4,5]

Metal–organic frameworks (MOFs) are microporous materials whose topologies and sorption properties can be more broadly tuned than classical mesoporous materials (*e.g.*, zeolites). MOFs are therefore among the most promising candidates for CO_2 capture and separation: their sorption selectivity to CO_2 with respect to many other common gases (*e.g.*, CH_4 and N_2) can be controlled by modulation of the micropore topology and volume, and by chemical functionalization of the pore surfaces.[4–7] In addition to size-exclusion mechanisms that favor the selective capture of CO_2 over larger molecules, thermodynamic separations can also be envisaged, whereby sorption selectivity is enhanced by promoting certain host–guest (*i.e.*, MOF-adsorbate) interactions.

Current synthetic approaches to achieve these aims include the incorporation of open metal sites that provide sites of stronger molecular sorption,[7] and by functionalizing the organic linker with Lewis basic groups (*e.g.*, amines, alcohols).[7,8] More recently, intensive studies are also being made to enhance the CO_2 uptake of MOFs by exploiting the synergis-

[a]*Laboratorio de Fisicoquímica y Reactividad de Superficies (LaFReS), Instituto de Investigaciones en Materiales, Universidad Nacional Autónoma de México, Circuito Exterior S/N, CU, Coyoacán, 04510 Ciudad de México, Mexico. E-mail: argel@unam.mx; Fax: +52(55) 5622-4595*

[b]*Institut Charles Gerhardt Montpellier, UMR-5253, Université de Montpellier, CNRS, ENSCM, Place E. Bataillon, 34095 Montpellier cedex 05, France. E-mail: guillaume.maurin@univ-montp2.fr*

[c]*Department of Chemistry, The University of Texas at Austin, Welch Hall 2.204, 105 East 24th St., Stop A5300, Austin, Texas 78712-1224, USA. E-mail: smh@cm.utexas.edu*

[d]*Departamento de Química, Universidad Autónoma Metropolitana-Iztapalapa, San Rafael Atlixco 186, Col. Vicentina, Iztapalapa, 09340 Ciudad de México, Mexico*

†Electronic supplementary information (ESI) available: TGA data, PXRD data water adsorption isotherm and kinetic CO_2 experiments. See DOI: 10.1039/c8dt03365j

‡These authors contributed equally to this work.

tic effects engendered by pre-confining small amounts of polar molecules in the pores.[9,10a,b] For example, Eddaoudi and co-workers[11] found that the recyclable and moisture-stable MOF SIFSIX-3-Cu could achieve enhanced CO_2 uptake and selectivity in highly diluted gas streams. Walton *et al.*[12] showed that pre-adsorption of sparing amounts of H_2O vapor inside MOFs decorated with hydroxyl functional groups in their pore walls led to a dramatic enhancement of the CO_2 uptake.[10c–e] In a similar fashion, we previously demonstrated that confinement of small amounts of H_2O in a series of MOFs consistently resulted in improved CO_2 capture properties.[13] Specifically, we found that μ_2-OH functional groups present in these MOFs (NOTT-400,[14] NOTT-401,[15] MIL-53(Al),[16] InOF-1[17]) can 'pin' H_2O adsorbates *via* relatively strong hydrogen bonding interactions.[13] These sequestered H_2O molecules are well ordered in the pore-structure of the MOFs and serve as preferential adsorption sites for subsequent CO_2 molecules.[18]

In related studies, Liu *et al.*[18d] and Chen *et al.*[18e] reported a moderate enhancement of the CO_2 uptake under 10% relative humidity (RH) in MIL-101 using experimental and computational approaches, respectively. Snurr and co-workers[18b] also provided a comprehensive simulation-analysis of the interactions between the quadrupole moment of gaseous CO_2 and the electric field created by H_2O molecules, which was the responsible for CO_2 capture enhancement in HKUST-1. LeVan *et al.*[18c] experimentally demonstrated that a small amount of H_2O increased the CO_2 adsorption capacity in the same material. More recently, Benoit *et al.* experimentally showed and corroborated by molecular simulations how the CO_2 adsorption properties were maintained for MIL-96(Al) under 10% RH.[10c]

In this context, our present study sought to explore the performance of an environmentally-friendly MOF Mg-CUK-1[19] (CUK for Cambridge University–KRICT), in the capture of CO_2 under humid conditions. This MOF can be considered to be environmentally-friendly, since it is rapidly synthesized under microwave-assisted heating in hydrothermal H_2O as the only solvent; it is also prepared using biologically-compatible Mg^{2+} ions and the low-toxicity organic ligand 2,4-pyridinedicarboxylate acid, $(NC_5H_3\text{-}2,4\text{-}(CO_2)_2)^{2-}$. The X-ray crystal structures of hydrated Mg-CUK-1 including positions of all H_2O solvates in the as-synthesized material, and its fully desolvated version have been published elsewhere; Mg-CUK-1 contains infinite 1-D rhombus-shaped microchannels with accessible openings of approximately 8.1 × 10.6 Å (see Fig. 1).[19] The Mg^{2+} centres in Mg-CUK-1 are octahedrally-coordinated as $[Mg_3(\mu_3\text{-}OH)]^{5+}$ triangles, which are bridged into infinite edge- and vertex-sharing 1-D chains that provide the MOF with structural robustness, even when the microchannels are devoid of guests. Besides this application-orientated exploration, advanced experimental and computational tools have allowed us to gain an unprecedented fundamental insight into the adsorption and co-adsorption mechanisms between H_2O and CO_2 in this MOF, which in turn help to explain the origins of CO_2 capture enhancement.

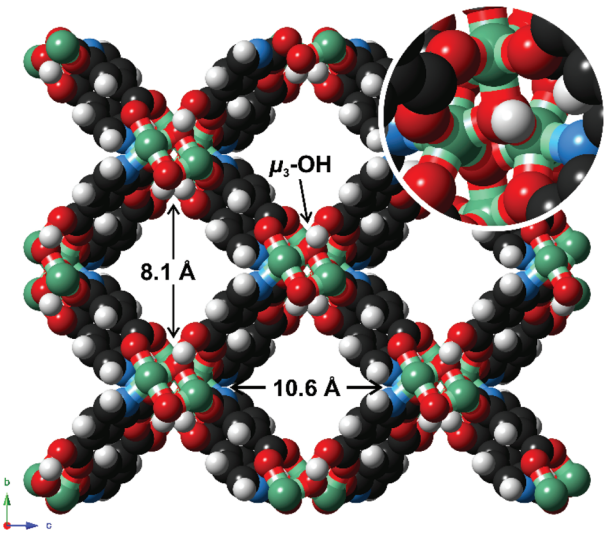

Fig. 1 Crystal structure of Mg-CUK-1 viewed along the crystallographic *a*-axis, depicting the one-dimensional channels with the hydroxyl group in the *b*-direction. Inset, trinuclear Mg(II) building block with the hydroxyl group pointing towards the center of the channel.

Experimental details

Chemicals

2,4-Pyridinedicarboxlic acid, magnesium nitrate hydrate ($Mg(NO_3)_2$) and potassium hydroxide (KOH) were obtained from Sigma-Aldrich and used as received.

Material synthesis

Mg-CUK-1 = $[Mg_3(OH)_2(2,4\text{-}PDC)_2$, 2,4-PCD = 2,4-pyridinecarboxylate], was synthesized following the previously reported procedure:[19] 2,4-Pyridinedicarboxlic acid (170 mg, 1.0 mmol) and KOH (2.0_M, 2.0 cm^3) in H_2O were added to a stirred solution of $Mg(NO_3)_2$, (380 mg, 1.5 mmol) in H_2O (3 cm^3) to give a viscous, opaque slurry mixture. The reaction mixture was placed inside a 23 cm^3 Teflon-lined autoclave and heated at 483 K for 15 h and then cooled down for 6 h. The crystalline solid was purified by short (3 × 20 s) cycles of sonication in fresh H_2O, followed by decanting of the slurry supernatant. Large, colorless prismatic crystals were isolated (average yield: 124 mg). TGA and PXRD were carried out and confirmed the nature of the synthesized material and its purity (see Fig. S1 and S2, respectively, ESI†).

Adsorption isotherms for CO_2 and H_2O

Ultra-pure grade (99.9995%) CO_2 gas was purchased from Praxair. CO_2 adsorption–desorption isotherms at 196 K and between 0–1 bar were carried out on a Belsorp mini II analyzer under high vacuum.

The calculated BET area ($0.01 < P/P_0 < 0.04$) based on the CO_2 adsorption data was approximately 600 $m^2\ g^{-1}$ with an associated pore volume of 0.21 $cm^3\ g^{-1}$. CO_2 adsorption–desorption isotherms were further collected up to 1 bar and 303 K on a Belsorp HP analyzer. An H_2O vapor isotherm was

recorded by a dynamic method in a DVS Advantage 1 instrument from Surface Measurement System (mass sensitivity: 0.1 μg; RH accuracy: 0.5% RH, vapor pressure accuracy: 0.7% P/P_0. Mg-CUK-1 samples were activated at 373 K for 1 hour under flowing N_2 prior to H_2O adsorption experiments.

Kinetic CO_2 capture experiments

Kinetic CO_2 uptake experiments were carried out on a thermobalance (Q500 HR, from TA) at room temperature (303 K) with a constant CO_2 flow (60 mL min^{-1}). Prior to these measurements, Mg-CUK-1 samples were placed inside the thermobalance and activated by heating from room temperature to 373 K for 1 h and under a N_2 gas flow. With the aid of a humidity-controlled thermobalance (Q5000 SA; TA Instruments), kinetic uptake experiments at 303 K with a constant CO_2 flow (60 mL min^{-1}) were carried out on activated Mg-CUK-1 samples. Additionally, these kinetic CO_2 experiments were performed in a DVS Advantage 1 instrument (Surface Measurement Systems; mass sensitivity: 0.1 μg, RH accuracy: 0.5% RH, vapor pressure accuracy: 0.7% P/P_0.

Computational details

The previously reported crystal structure of Mg-CUK-1[19] was geometrically optimized at the density functional theory (DFT) level while keeping the experimental cell parameters fixed. Calculations employed the PBE functional[20] combined with a double numeric basis set containing polarization functions (DNP)[21] as implemented in the Dmol^3 package. The partial charges of each atom of the Mg-CUK-1 framework were derived using an ESP fitting strategy applied to a cluster model cleaved from the periodic structure (see ESI†). The 12–6 Lennard-Jones (LJ) parameters of the inorganic and organic moieties of the MOF were taken from the UFF[24] and DREIDING[25] force fields, respectively. Following a general approach adopted in previous studies,[26] the hydrogen of the μ_3-OH groups interacts with the guests only through electrostatic interactions.

The microscopic models of the two guest molecules were defined as follows: (i) CO_2 was described by the EPM2 model[22] corresponding to 3 charged Lennard-Jones (LJ) sites centered on the atoms of CO_2; and, (ii) H_2O was represented by the TIP4P/2005 model[23] (a 4-site model) with 1 LJ site centered in the oxygen position and 3 charged sites, two centered in the hydrogen positions, and one situated 0.1546 Å below the oxygen atom in the molecular bisector axis.

Grand Canonical Monte Carlo (GCMC) simulations were carried out at 303 K to predict the adsorption behavior of Mg-CUK-1or H_2O and CO_2 as single components. We employed a simulation box comprised of 12-unit cells (3 × 2 × 2), maintaining all atoms of the framework in their initial positions. The Mg-CUK-1/guest interactions were described by a 6–12 LJ potential and a coulombic contribution. The LJ crossed parameters between the MOF and the guests were calculated using the Lorentz–Berthelot mixing rules. The LJ contribution was evaluated using a cut-off distance of 12 Å while the long-range electrostatic interactions were accounted for using the Ewald summation technique.[27] The adsorption enthalpies at low coverage for each single guest were calculated using the revised Widom's test particle insertion method.[28] As a further step, in order to gain insight on the CO_2 adsorption properties of Mg-CUK-1 in the presence of H_2O, GCMC were performed for a MOF loaded with 1 molecule of H_2O per unit cell, which gives a good approximation to the experimental uptake, *i.e.*, 0.99 wt% H_2O loading (corresponding to that of 18% RH).

Additional Monte Carlo simulations were performed in the NVT ensemble to identify the preferential adsorption sites for the guest molecules at low, intermediate and high pressures for the single components. This exploration implied the analysis of radial distribution functions plotted between different MOF/guest pairs, energy histograms and center of mass (COM) density plots calculated from hundreds of MC configurations.

Results and discussion

Experimental

Fig. 2 reports the H_2O adsorption isotherm for Mg-CUK-1 measured between % P/P_0 = 0–95 at 303 K. As previously reported,[29] Mg-CUK-1 proved to be water-stable and eight H_2O adsorption–desorption cycles were also performed at 303 K, (see Fig. S3, ESI†). In addition, PXRD experiments confirmed the water-stability (see Fig. S4, ESI†) of Mg-CUK-1 after the H_2O sorption isotherm (*vide infra*).

The experimental static CO_2 adsorption isotherm (thermodynamic analysis, see Fig. 3) first demonstrated an enhancement of the CO_2 capture in the presence of 18% RH. Following this observation, we decided to further investigate the kinetic evolution of CO_2 uptake (CO_2 capture *versus* time) as a function of H_2O content over the range 5–20% RH. These RH values were selected based on the H_2O adsorption isotherm (see Fig. 2), since they are located in the lower H_2O uptake region, where the uptake slowly increases with increasing % P/P_0. With this in mind, kinetic CO_2 experiments were first

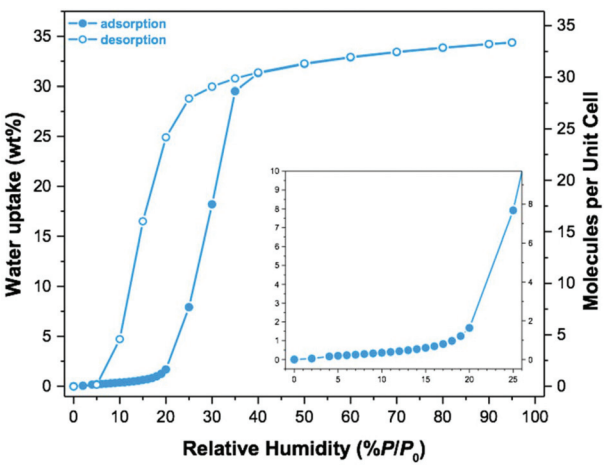

Fig. 2 Water adsorption isotherm of Mg-CUK-1 at 303 K from % P/P_0 = 0 to 95, the inset shows water loadings range from % P/P_0 = 0 to 25.

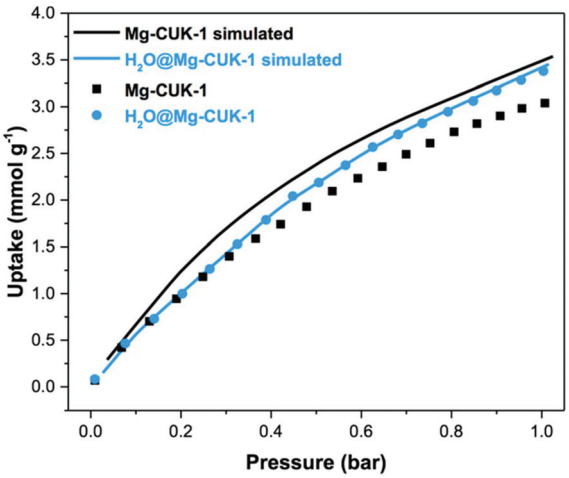

Fig. 3 CO_2 adsorption isotherm at 303 K for fully dehydrated Mg-CUK-1 (black squares) and Mg-CUK-1 in the presence of 18% RH (blue circles); the corresponding simulated adsorption isotherms are represented as solid lines.

performed at 303 K with a constant CO_2 flow of 60 mL min^{-1} (Fig. 4).

Under anhydrous conditions and 303 K, the maximum CO_2 capture was estimated to be 4.6 wt%, which was reached after only 10 min; after this period of time, the CO_2 loading remained constant (30 min). Next, a kinetic CO_2 isotherm experiment at 303 K was carried out under the same range of RH values. Table 1 and Fig. 4 showed the corresponding CO_2 experiments' kinetic results under different relative humidities. These kinetic results confirmed that at 18% RH, the CO_2 capture was considerably enhanced to a maximum CO_2 uptake (see Table 1 and Fig. 4) that is internally consistent with the prior thermodynamics observations.

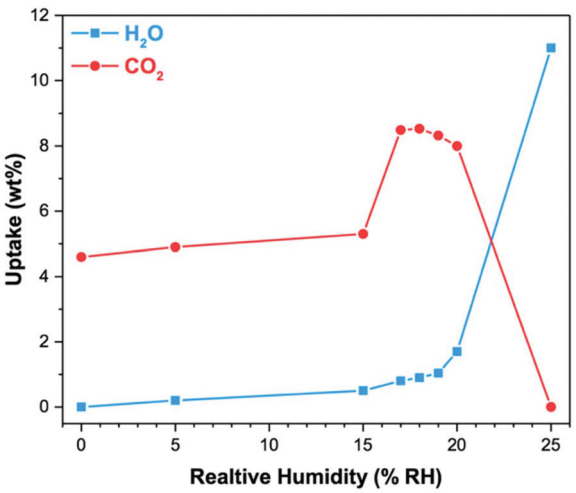

Fig. 4 Mg-CUK-1 individual uptake of pre-adsorbed H_2O and CO_2 capture (from kinetic experiments) for different relative humidities at 303 K.

Table 1 Uptake data from the kinetic CO_2 isotherm experiments at 303 K at different relative humidities

	Uptake (wt%)		Molecules per unit cell		Molecules per μ_3-OH group	
Relative humidity (RH%)	H_2O	CO_2	H_2O	CO_2	H_2O	CO_2
0	—	4.6	—	1.827	—	0.228
5	0.2	4.9	0.194	1.946	0.024	0.243
15	0.5	5.3	0.485	2.105	0.061	0.263
17	0.8	8.49	0.776	3.372	0.097	0.422
18	0.9	8.53	0.874	3.388	0.109	0.424
19	1.04	8.32	1.009	3.305	0.126	0.413
20	1.7	8	1.650	3.178	0.206	0.397

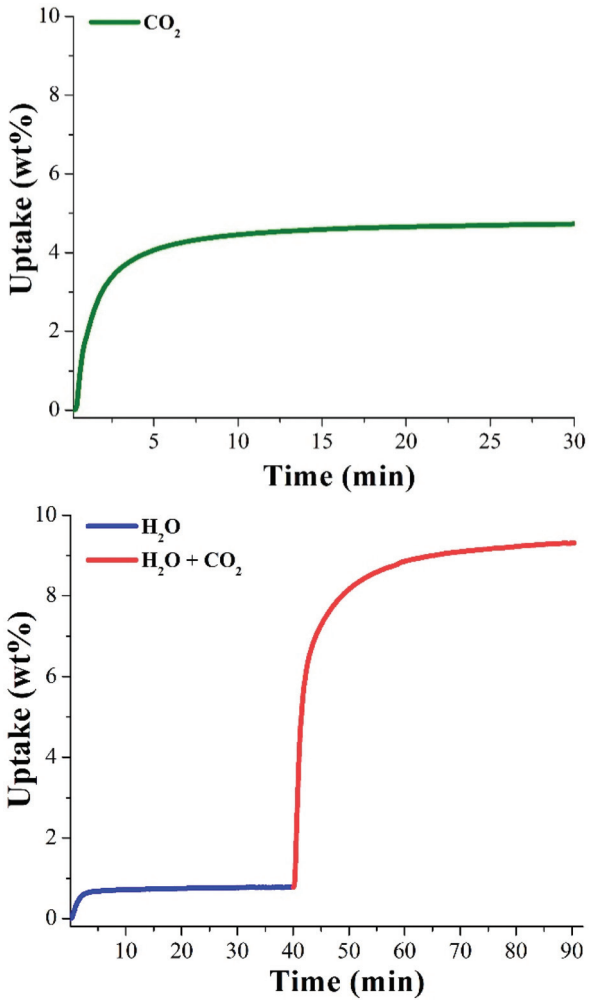

Fig. 5 (Top) Kinetic CO_2 uptake experiment performed at 303 K with a CO_2 flow of 60 mL min^{-1}; (bottom) kinetic CO_2 uptake experiments carried out at 18%RH at 303 K; H_2O (blue line) and H_2O + CO_2 (red line).

Fig. 5 (bottom) reports the kinetic CO_2 adsorption at constant % RH in two distinct regimes: (i) the pre-adsorption of only H_2O (see Fig. 4, right-blue line); and, (ii) the CO_2 adsorption in the presence of this H_2O within the pore of Mg-CUK-1

(see Fig. 5, bottom-red line). When we imposed 18%RH (only adsorption of H_2O), the sample weight rapidly increased (Fig. 5, bottom; blue data). A steady-state with respect to CO_2 loading was achieved after 10 min and was fully stabilized at ~20 min. Then, from 20 min to 40 min the H_2O uptake remained constant at 0.9 wt%, which is consistent with the H_2O uptake obtained from the adsorption isotherm at 303 K (0.99 wt%, see Fig. 2). At 40 min, CO_2 flow (60 mL min^{-1}) was initiated, resulting in a rapid weight increase (H_2O + CO_2), which reached stability at approximately 70 min, (Fig. 5, bottom; red data). Then, the maximum amount of CO_2 captured (considering the H_2O uptake of 0.9 wt%) was equal to 8.5 wt%. Ultimately, CO_2 capture by Mg-CUK-1 in the presence of 18% RH was increased by a factor of 1.8 due to the presence of favorable CO_2···H_2O interactions inside the microchannels (from 4.6 wt% to 8.5 wt%).

This magnitude was confirmed by performing kinetic CO_2 experiments in a DVS Advantage 1 instrument (SMS). This equipment has a much higher measurement sensitivity, enabling H_2O pre-adsorption in Mg-CUK-1 to be completed in 20 min timeframe (Fig. S5†), resulting in a total H_2O capture of approximately 0.85 wt%. Subsequently, CO_2 adsorption (60 mL min^{-1}) was recorded from 20 min to the end of the experiment (160 min), to reach a total CO_2 capture of ~8.4 wt% (Fig. S5†). Thus, the enhancement of the CO_2 uptake in the presence of humidity was even more pronounced in the case of the breakthrough curves (kinetic analysis) than at the thermodynamic level.

Molecular simulations

The simulated H_2O adsorption isotherm for Mg-CUK-1 was first compared to the corresponding experimental data. Close agreement between the two sets of data over the entire pressure range provided validation of the microscopic models for both Mg-CUK-1 (LJ parameters and charges) and H_2O, to accurately reproduce the adsorption behavior in this MOF. This is also supported when the consideration of the fully desolvated MOF in the whole range of water relative pressure is a reasonable approximation to capture the water adsorption behavior of Mg-CUK-1. We have evidenced that H_2O preferentially interacts with the hydroxyl groups that project into the MOF microchannels, while only a small fraction of adsorbed H_2O is located in the vicinity of the organic linker as illustrated by the Center-of-Mass density plot calculated for 1 H_2O per u.c. (see Fig. 6).

The experimental CO_2 adsorption isotherm (from 0 to 1 bar and 303 K, see Fig. 3) was also very well reproduced by our GCMC simulations, which indicated a relatively high adsorption enthalpy of −35 kJ mol^{-1}; this magnitude is in-line with what has been reported elsewhere for interactions between CO_2 and MOFs containing hydroxyl groups.[30] Analysis of the configurations generated by our MC simulations at low

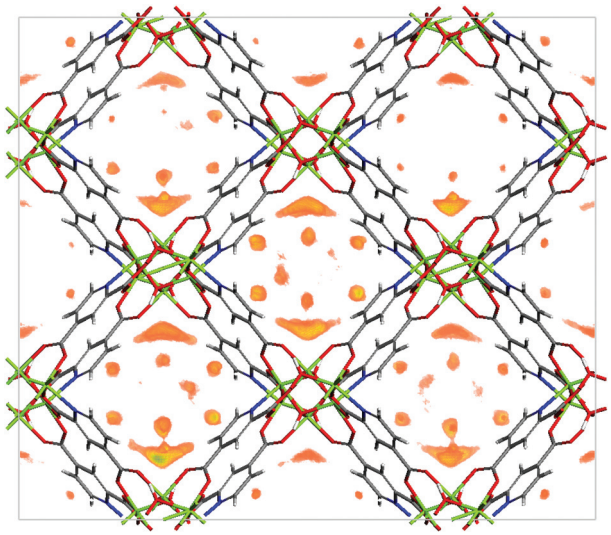

Fig. 6 Center of mass distribution of H_2O in Mg-CUK-1 calculated by Monte Carlo simulations considering the case of 1 H_2O molecule per u.c. at 303 K.

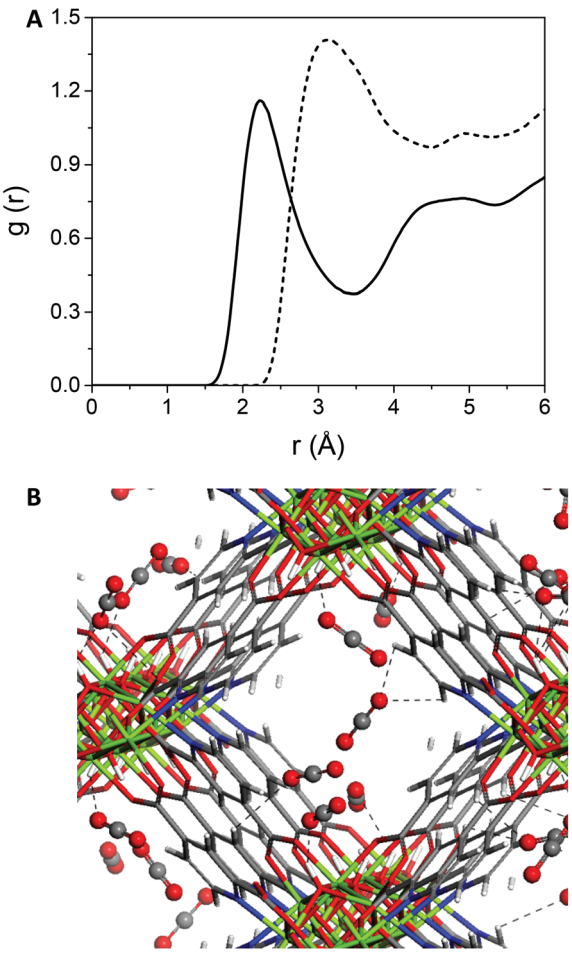

Fig. 7 A. Radial distribution functions calculated by GCMC simulations at 1 bar and 303 K for the pairs O_{CO_2}···$H_{\mu_3\text{-}OH}$ (solid line) and O_{CO_2}···H_{PDC} (dashed line) for Mg-CUK-1. B. Representative snapshot illustrating the interactions between CO_2 and the atoms of the MOF pore wall. The dashed lines in the snapshots denote interactions between the CO_2 molecules and the surrounding atoms at distances bellow 3 Å.

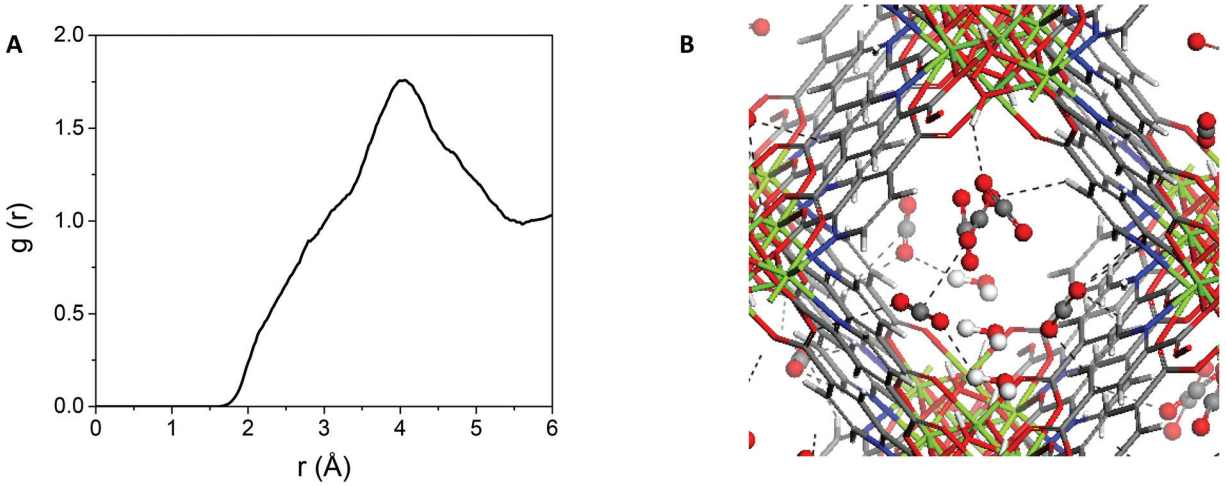

Fig. 8 A. Radial distribution functions calculated by GCMC simulations at 1 bar and 303 K for the pair O_{CO_2}–H_w for hydrated Mg-CUK-1. B. Representative snapshot showing the interactions between CO_2 and the atoms of the MOF pore wall. The dashed lines in the snapshots denote interactions between the CO_2 molecules and the surrounding atoms at distances bellow 3 Å.

loading indicated that the CO_2 molecules predominantly interact with the hydroxyl groups, and to a lesser extent with the conjugated organic moieties. This is supported by RDFs plots of the corresponding pairs (Fig. 7A), which show that the average distances between the oxygen of CO_2 (O_{CO_2}), the hydrogen of the hydroxyl groups (H_{OH}) and the hydrogen of the organic linkers (H_{PDC}) are 2.2 and 3.1 Å respectively. These overall host/guest interactions are illustrated by a representative MC snapshot reported in Fig. 7B.

As a further step, our simulations confirmed a slight enhancement of the CO_2adsorption uptake for the H_2O loaded Mg-CUK-1 (18% RH) as compared to the pristine Mg-CUK-1 (see Fig. 3). In the presence of humidity, GCMC simulations evidenced that the CO_2 molecules interact, not only with the sites described above, but also with the H_2O molecules, as shown in the snapshot in Fig. 8B. However, such $H_2O\cdots CO_2$ interactions are relatively weak as revealed by the RDF plot for the corresponding pair (Fig. 8A), which shows that the most preferential interacting distances are above 3 Å. This observation is also supported by a relatively small increase of the CO_2 adsorption enthalpy at low coverage in the presence of H_2O (−36.5 kJ mol^{-1}) *vs.* the anhydrous scenario (−35 kJ mol^{-1}).

Conclusions

Kinetic CO_2 uptake experiments revealed a significant enhancement of the CO_2 capture performances for the water-stable MOF Mg-CUK-1, *i.e.*, a 1.8-fold increase (from 4.6 wt% to 8.5 wt% CO_2 uptake) under 18% RH. This trend was also confirmed by thermodynamic measurements and GCMC simulations. The phenomenon of H_2O-induced CO_2 uptake enhancement was highly pronounced in measurements conducted under thermodynamic control. The underlying kinetics responsible for this process are more difficult to understand and measure directly, but supporting molecular simulations allowed us to gain additional insights into the microscopic adsorption mechanisms at play. In particular, theory suggests that an increase in the CO_2 adsorption enthalpy, in the presence of H_2O, is due to favorable intermolecular interactions between CO_2 and H_2O which are confined within Mg-CUK-1. The fundamental understanding gained from this joint experimental/computation study paves the way towards the design of new and more efficient CO_2 capture systems under humid (*i.e.*, realistic, ambient) conditions.

Conflicts of interest

There are no conflicts of interest.

Acknowledgements

The authors thank Dr A. Tejeda-Cruz (powder X-ray; IIM-UNAM), CONACyT Mexico (1789), PAPIIT UNAM Mexico (IN101517) for financial support. E. G-Z. thanks CONACyT (236879), Mexico for financial support. Thanks to U. Winnberg (ITAM) and G. Ibarra-Winnberg for scientific discussions. P. G. M. Mileo thanks the National Counsel of Technological and Scientific Development (CNPQ) for the scholarship. G. M. thanks the Institut Universitaire de France for its support. E. S.-G. thanks CONACyT Mexico (grant no. 289042).

Notes and references

1 National Oceanic and Atmospheric Administration (NOAA), https://www.esrl.noaa.gov/gmd/ccgg/trends/?utm_source=www.uoota.com (accessed[:] May 30, 2018).

2 Intergovernmental Panel on Climate Change (IPCC), https://www.ipcc.ch/publications_and_data/publications_ipcc_fourth_assessment_report_wg1_report_the_physical_science_basis.htm (accessed may 30, 2018).
3 (*a*) I. S. Thakura, M. Kumara, S. J. Varjanib, Y. Wuc, E. Gnansounoud and S. Ravindrane, *Bioresour. Technol.*, 2018, **256**, 478–490; (*b*) M. H. Ibrahim, M. H. El-Naas, Z. Zhang and B. Van der Bruggen, *Energy Fuels*, 2018, **32**, 963–978.
4 (*a*) S. L. James, *Chem. Soc. Rev.*, 2003, **32**, 276–288; (*b*) J. L. C. Rowsell and O. M. Yaghi, *Microporous Mesoporous Mater.*, 2004, **73**, 3–14; (*c*) S. Choi, J. H. Drese and C. W. Jones, *ChemSusChem*, 2009, **2**, 796–854; (*d*) J. Wang, L. Huang, R. Yang, Z. Zhang, J. Wu, Y. Gao, Q. Wang, D. O'Hareb and Z. Zhong, *Energy Environ. Sci.*, 2014, **7**, 3478–3518; (*e*) B. Dou, C. Wang, Y. Song, H. Chen, B. Jiang, M. Yang and Y. Xu, *Renewable Sustainable Energy Rev.*, 2016, **53**, 536–546.
5 N. M. Padial, E. Quartapelle Procopio, C. Montoro, E. López, J. E. Oltra, V. Colombo, A. Maspero, N. Masciocchi, S. Galli, I. Senkovska, S. Kaskel, E. Barea and J. A. R. Navarro, *Angew. Chem., Int. Ed.*, 2013, **52**, 8290–8294.
6 (*a*) S.-L. Li and Q. Xu, *Energy Environ. Sci.*, 2013, **6**, 1656–1683; (*b*) V. Bon, *Curr. Opin. Green Sustain. Chem.*, 2017, **4**, 44–49.
7 (*a*) M. Dincă and J. R. Long, *Angew. Chem., Int. Ed.*, 2008, **47**, 6766–6779; (*b*) K. M. Thomas, *Dalton Trans.*, 2009, **9**, 1487–1505; (*c*) H. W. Langmi, J. Ren, B. North, M. Mathe and D. Bessarabov, *Electrochim. Acta*, 2014, **128**, 368–392.
8 (*a*) K. Sumida, D. L. Rogow, J. A. Mason, T. M. McDonald, E. D. Bloch, Z. R. Herm, T.-H. Bae and J. R. Long, *Chem. Rev.*, 2012, **112**, 724–781; (*b*) J. Liu, P. K. Thallapally, B. P. McGrail, D. R. Brown and J. Liu, *Chem. Soc. Rev.*, 2012, **41**, 2308–2322; (*c*) D. Andirova, C. F. Cogswell, Y. Lei and S. Choi, *Microporous Mesoporous Mater.*, 2016, **219**, 276–305; (*d*) D. Y. Hong, Y. K. Hwang, C. Serre, G. Férey and J. S. Chang, *Adv. Funct. Mater.*, 2009, **19**, 1537–1552; (*e*) W. Bloch, R. Babarao, M. R. Hill, C. J. Doonan and C. Sumby, *J. Am. Chem. Soc.*, 2013, **135**, 10441–10448.
9 (*a*) J. J. Low, A. I. Benin, P. Jakubczak, J. F. Abrahamian, S. A. Faheem and R. R. Willis, *J. Am. Chem. Soc.*, 2009, **5**, 15834–15842; (*b*) J. Canivet, A. Fateeva, Y. Guo, B. Coasne and D. Farrusseng, *Chem. Soc. Rev.*, 2014, **43**, 5594–5617; (*c*) J. Canivet, J. Bonnefoy, C. Daniel, A. Legrand, B. Coasne and D. Farrusseng, *New J. Chem.*, 2014, **38**, 3102–3111.
10 (*a*) M. R. Gonzalez, J. H. Gonzalez-Estefan, H. A. Lara-Garcia, P. Sanchez-Camacho, E. I. Basaldella, H. Pfeiffer and I. A. Ibarra, 2015, **39**, 2400–2403; (*b*) H. A. Lara-García, M. R. Gonzalez, J. H. González-Estefan, P. Sánchez-Camacho, E. Lima and I. A. Ibarra, *Inorg. Chem. Front.*, 2015, **2**, 442–447; (*c*) V. Benoit, N. Chanut, R. S. Pillai, M. Benzaqui, I. Beurroies, S. Devautour-Vinot, C. Serre, N. Steunou, G. Maurin and P. L. Llewellyn, *J. Mater. Chem. A*, 2018, **6**, 2081–2090; (*d*) M. Benzaqui, R. S. Pillai, A. Sabetghadam, V. Benoit, P. Normand, J. Marrot, N. Menguy, D. Montero, W. Shepard, A. Tissot, C. Martineau-Corcos, C. Sicard, M. Mihaylov, F. Carn, I. Beurroies, P. L. Llewellyn, G. De Weireld, K. Hadjiivanov, J. Gascon, F. Kapteijn, G. Maurin, N. Steunou and C. Serre, *Chem. Mater.*, 2017, **29**, 10326–10338; (*e*) J. W. Yoon, Y. K. Seo, Y. K. Hwang, J. S. Chang, H. Leclerc, S. Wuttke, P. Bazin, A. Vimont, M. Daturi, E. Bloch, P. L. Llewellyn, C. Serre, P. Horcajada, J. M. Grenèche, A. E. Rodrigues and G. Férey, *Angew. Chem., Int. Ed.*, 2010, **49**, 5949–5952.
11 P. Nugent, Y. Belmabkhout, S. D. Burd, A. J. Cairns, R. Luebke, K. Forrest, T. Pham, S. Ma, B. Space, L. Wojtas, M. Eddaoudi and M. J. Zaworotko, *Nature*, 2013, **495**, 80–84.
12 (*a*) H. Jasuja, Y. G. Huang and K. S. Walton, *Langmuir*, 2012, **28**, 16874–16880; (*b*) H. Jasuja, J. Zang, D. S. Sholl and K. S. Walton, *J. Phys. Chem. C*, 2012, **116**, 23526–23532; (*c*) J. B. DeCoste, G. W. Peterson, H. Jasuja, T. G. Glover, Y. Huang and K. S. Walton, *J. Mater. Chem. A*, 2013, **1**, 5642; (*d*) P. M. Schoenecker, C. G. Carson, H. Jasuja, C. J. J. Flemming and K. S. Walton, *Ind. Eng. Chem. Res.*, 2012, **51**, 6513–6519; (*e*) N. C. Burtch, H. Jasuja and K. S. Walton, *Chem. Rev.*, 2014, **114**, 10575–10612; (*f*) G. E. Cmarik, M. Kim, S. M. Cohen and K. S. Walton, *Langmuir*, 2012, **28**, 15606–15613.
13 E. González-Zamora and I. A. Ibarra, *Mater. Chem. Front.*, 2017, **1**, 1471–1484.
14 J. R. Álvarez, R. A. Peralta, J. Balmaseda, E. González-Zamora and I. A. Ibarra, *Inorg. Chem. Front.*, 2015, **2**, 1080–1084.
15 E. Sánchez-González, J. R. Álvarez, R. A. Peralta, A. Campos-Reales-Pineda, A. Tejeda-Cruz, E. Lima, J. Balmaseda, E. González-Zamora and I. A. Ibarra, *ACS Omega*, 2016, **1**, 305–310.
16 M. Sánchez-Serratos, P. A. Bayliss, R. A. Peralta, E. González-Zamora, E. Lima and I. A. Ibarra, *New J. Chem.*, 2016, **40**, 68–72.
17 R. A. Peralta, B. Alcántar-Vázquez, M. Sánchez-Serratos, E. González-Zamora and I. A. Ibarra, *Inorg. Chem. Front.*, 2015, **2**, 898–903.
18 (*a*) H. Wu, Q. Gong, D. H. Olson and J. Li, *Chem. Rev.*, 2012, **112**, 836–868; (*b*) A. Ö. Yazaydin, A. I. Benin, S. A. Faheem, P. Jakubczak, J. J. Low, R. W. Richard and R. Q. Snurr, *Chem. Mater.*, 2009, **21**, 1425–1430; (*c*) J. Liu, Y. Wang, A. I. Benin, P. Jakubczak, R. R. Willis and M. D. LeVan, *Langmuir*, 2010, **26**, 14301–14307; (*d*) Q. Liu, L. Ning, S. Zheng, M. Tao, Y. Shi and Y. He, *Sci. Rep.*, 2013, **3**, 2916–2921; (*e*) Y. F. Chen, R. Babarao, S. I. Sandler and J. W. Jiang, *Langmuir*, 2010, **26**, 8743–8750.
19 B. Saccoccia, A. M. Bohnsack, N. W. Waggoner, K. H. Cho, J. S. Lee, D. Y. Hong, V. M. Lynch, J. S. Chang and S. M. Humphrey, *Angew. Chem., Int. Ed.*, 2015, **54**, 5394–5398.
20 J. P. Perdew, K. Burke and M. Ernzerhof, *Phys. Rev. Lett.*, 1996, **77**, 3865–3868.
21 W. J. Hehre, J. A. Ditchfield and J. A. Pople, *J. Chem. Phys.*, 1972, **56**, 2257–2261.
22 J. G. Harris and K. H. Yung, *Phys. Chem.*, 1995, **99**, 12021–12024.
23 J. L. F. Abascal and C. A. Vega, *J. Chem. Phys.*, 2005, **123**, 234505–234512.

24 A. K. Rappe, C. J. Casewit, K. S. Colwell, W. A. Goddard and W. M. Skiff, *J. Am. Chem. Soc.*, 1992, **114**, 10024–10035.
25 S. L. Mayo, B. D. Olafson and W. A. Goddard, *J. Phys. Chem.*, 1990, **94**, 8897–8909.
26 (*a*) E. Sanchez-Gonzalez, P. G. M. Mileo, J. J. R. Alvarez, E. Gonzalez-Zamora, G. Maurin and I. A. Ibarra, *Dalton Trans.*, 2017, **46**, 15208–15215; (*b*) D. D. Borges, P. Normand, A. Permiakova, R. Babarao, N. Heymans, D. S. Galvão, C. Serre, G. Weireld and G. Maurin, *J. Phys. Chem. C*, 2017, **121**, 26822–26832.
27 (*a*) O. N. Osychenko, G. E. Astrakharchik and J. Boronat, *Mol. Phys.*, 2012, **110**, 227–247; (*b*) J. Kolafa and J. W. Perram, *Mol. Simul.*, 1992, **9**, 351–368.
28 T. J. H. Vlugt, E. García-Perez, D. Dubbeldam, S. Ban and S. Calero, *J. Chem. Theory Comput.*, 2008, **4**, 1107–1118.
29 E. Sánchez-González, P. G. M. Mileo, M. Sagastuy-Breña, J. R. Álvarez, J. E. Reynolds, A. Villarreal, A. Gutiérrez-Alejandre, J. Ramírez, J. Balmaseda, E. González-Zamora, G. Maurin, S. M. Humphrey and I. A. Ibarra, *J. Mater. Chem. A*, 2018, **6**, 16900–16909.
30 (*a*) D.-M. Chen, X.-P. Zhang, W. Shi and P. Cheng, *Inorg. Chem.*, 2015, **54**, 5512; (*b*) G. E. Cmarik, M. Kim, S. M. Cohen and K. S. Walton, *Langmuir*, 2012, **28**, 15606; (*c*) D.-M. Chen, N.-N. Zhang, C.-S. Liu, Z.-H. Jiang, X.-D. Wang and M. Du, *Inorg. Chem.*, 2017, **56**, 2379.